PEKAN 1: Performance evaluation of an autonomous solar-powered device for repelling birds and wild animals

Andrei FOCA

Department of Electronic Devices, Circuits and Architectures (DCAE), Faculty of Electronics, Telecommunications and Information Technology, National University of Science and Technology POLITEHNICA Bucharest, Bucharest, Romania

focaandrei30@gmail.com

Abstract: Electrical bird and wildlife deterrents have existed for many years, yet there remains a practical gap between inexpensive static devices and costly professional systems. This paper evaluates PEKAN 1, an autonomous solar-powered animatronic scarecrow intended for small gardens and hobby agricultural use. The device combines on-device object detection, a rotating mechanical body, a Class-D acoustic deterrent, infrared night illumination, and a LiFePO4 battery system charged from a solar panel. Tests focused on the factors that determine whether the prototype is usable in the field: day and night detection range, acoustic level estimation, raw audio storage, passive cell balancing, overcurrent protection, overdischarge cut-off, and solar charging behavior under good and poor irradiation conditions. The prototype detected the validation target up to 9 m in daylight and 4 m at night, balanced an intentionally unbalanced 5S pack in approximately 52 h, and reached practical charge and protection values close to those predicted by the theoretical design, thereby confirming the main architecture. The results show a functional minimum viable product, while also identifying weatherproofing, night illumination, and mechanical durability as the main areas for improvement.

Keywords: Animatronic scarecrow, Object detection, Bird deterrence, Solar charging.

PEKAN 1: Evaluarea performanței unui dispozitiv autonom, alimentat cu energie solară, pentru îndepărtarea păsărilor și a animalelor sălbatice

Rezumat: Dispozitivele electrice pentru îndepărtarea păsărilor și a animalelor sălbatice există de mulți ani, însă între soluțiile statice ieftine și sistemele profesionale costisitoare rămâne un segment practic insuficient acoperit. Această lucrare evaluează PEKAN 1, o sperietoare animatronică autonomă, alimentată cu energie solară, destinată grădinilor mici și utilizării agricole de tip hobby. Dispozitivul combină detecția locală a obiectelor, un corp mecanic rotativ, un sistem acustic de descurajare, iluminare în infraroșu pentru utilizarea pe timp de noapte și un acumulator LiFePO4 încărcat de la un panou solar. Testele au urmărit elementele care determină utilitatea prototipului în teren: raza de detecție zi/noapte, estimarea nivelului acustic, stocarea audio brută, echilibrarea pasivă a celulelor, protecția la supracurent, oprirea la supradescărcare și comportamentul încărcătorului solar în condiții bune și slabe de iradiere. Prototipul a detectat ținta de validare până la 9 m ziua și 4 m noaptea, a echilibrat un pachet 5S dezechilibrat intenționat în aproximativ 52 h și a confirmat funcționarea arhitecturii principale prin valori practice apropiate de cele rezultate din proiectarea teoretică. Rezultatele indică un produs minim viabil funcțional și identifică, totodată, etanșarea la intemperii, iluminarea nocturnă și durabilitatea mecanică drept principalele direcții de îmbunătățire.

Cuvinte-cheie: sperietoare animatronică, detecția obiectelor, îndepărtarea păsărilor, încărcare solară.

1. Introduction

Bird and predator repellent props and devices have long been available on the market, but their reported efficiency differs widely from one product category to another. At the low-cost end of the spectrum, there are reflective tapes and static visual objects, whose purpose is either to create visual discomfort or to resemble a natural predator. Going further, there are inexpensive solar ultrasonic devices and then stronger auditory deterrents, such as loudspeaker systems or propane/gas cannons. Reviews of bird-scaring methods repeatedly point out that visual and acoustic tools are strongly dependent on context, timing and variation, and that no single deterrent is a universal solution (Bishop et al., 2003; USDA APHIS, 2026). At the professional end of the

https://doi.org/10.33436/v36i3y202608

spectrum, laser-based systems can operate with less acoustic disturbance by tracking and aiming a beam at a valid target, but their price moves them into a different product category.

This leaves a visible gap in the middle. The major downside of many affordable consumer tools is their predictability. Crows and ravens are intelligent enough to habituate to a fixed stimulus, especially when the stimulus is not tied to their own presence (Bishop et al., 2003; Minnesota Department of Natural Resources, n.d.). Unless smart detection is used, playing predator sounds after a random time interval only teaches the animals that the device operates regardless of where they are. The next logical step is therefore the addition of object detection to a traditional sound-based scarecrow. This is how the idea of the project arose, as shown in Figures 1 and 2, and because the target use case includes gardens without grid access, a solar-powered battery system became mandatory.

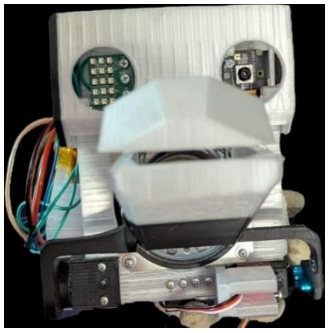


Figure 1. PEKAN 1 Front View

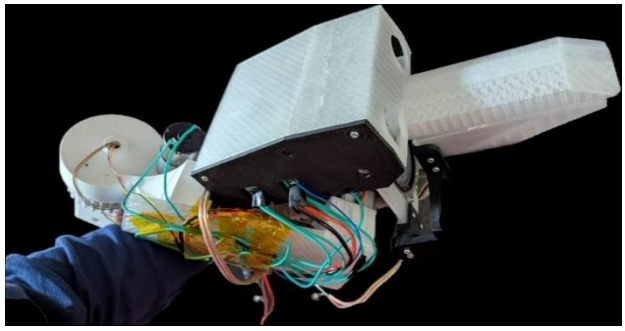


Figure 2. PEKAN 1 Angle View

(Source: Author's own research)

From this point onward, this article focuses primarily on the hobbyist agricultural applicability of the PEKAN 1; nonetheless, the intended final target of the device can be extended thanks to the flexible nature of object detection models and transfer learning workflows. YOLO11 was selected because the model family is designed for real-time detection and provides a practical balance between accuracy, speed and edge deployment support (Ultralytics, 2024). The final detection behavior is still influenced by the physical size and appearance of the target. Nevertheless, the detection range may vary between species because target size, pose, contrast and visual similarity strongly influence object-detection performance. Additional use cases are discussed later in the article.

The remainder of this paper is organized as follows. Section 2 reviews related work on electronic deterrents, focusing on ultrasonic repellent devices and on evidence regarding their effectiveness against birds. Section 3 presents the architecture of the device, with detailed descriptions of the Logic, Control Buffer and Power blocks. Section 4 reports the experimental evaluation of the detection range, using a 3D-printed crow model as the validation target, and of the power PCB parameters. Section 5 briefly describes the firmware of the STM32-based buffer PCB, the power PCB and the Raspberry Pi 5. Section 6 discusses the differences between theoretical and measured values, the current limitations of the prototype, and possible solutions for operation under real-world field conditions. Section 7 outlines the improvements planned for a future version, and Section 8 presents the conclusions.

2. Related work

The electronic deterrents described in the literature are dominated by frequency generation architectures, in which ultrasonic frequencies are employed. The review conducted by Tiwari & Ansari (2016) covers a broad set of such implementations, the majority of them being built around the 555 timer or NE555 oscillator, a CD4017 decade counter and a push-pull output stage operating between 10 and 100 kHz. The results collected are encouraging but vary across publications. One reviewed device was credited with around 75% efficiency against insects, another was trialed against mice at 5, 10 and 15 m respectively, while a third was reported to cover a diameter of approximately 16 m. The same review acknowledges the influence that factors such as humidity and temperature have on the range of such devices.

A recent implementation based on the same functional architecture is the solar-powered ultrasonic rodent repellent for poultry farms proposed by Hema (2022). At the power level, the architecture is close to the PEKAN 1 – it uses the same implementation of a photovoltaic panel, rechargeable battery, regulator and microcontroller, but its deterrent stage differs, having an Arduino-generated square wave amplified by an LM386 into an 8-ohm transducer, with operating frequency options including 20 kHz to 100 kHz. Validation consisted of a single caged rat exposed to the 60-85 kHz band, with reaction times of 10 s at 1 m and 15 s at 2 m when operating at 70 kHz, improving to 3 s and 5 s respectively at 85 kHz. The reported autonomy is approximately 12 h on a full charge.

There are two operational differences between these systems and the PEKAN 1. The first is the control policy, where both the devices surveyed by Tiwari & Ansari (2016) and the prototype of Hema (2022) are open-loop – the emitter runs continuously or on an operator command, regardless of whether a valid target is present. The PEKAN 1 is closed-loop, releasing its acoustic and mechanical response only upon a continuous one-second target detection.

The second difference concerns the target species. Both studies address rodents and insects, and although Tiwari & Ansari (2016) state that their technique extends to birds, no avian audiometric evidence is cited to support that extension. The ornithological literature also does not support their claim: Beason (2004) reports that no bird species tested has shown sensitivity to frequencies above 20 kHz, avian hearing being most acute between about 1 kHz and 4 kHz, while the review of frightening devices by Gilsdorf, Hygnstrom & VerCauteren (2002) concludes that ultrasonic devices are ineffective in repelling birds.

However, what can be compared directly is the range. The ultrasonic devices were validated at short distances: 1 and 2 m in Hema (2022), and 5 to 15 m in the trials reviewed by Tiwari & Ansari (2016). These are roughly the same order of magnitude as the 9 m daylight and 4 m nighttime detection ranges measured in this paper. The difference is that the PEKAN 1 is limited by its camera and not by its speaker, as the free-field estimate in Section 3.2 places the acoustic stage range at around 19 m. Duttenhefner & Klug (2024) derive the effective frightening range for nuisance blackbirds from published audiograms and observed antipredator responses, which is a stricter method than the free-field estimate used here. Habituation is another common point. Tiwari & Ansari (2016) name the predictability of a fixed stimulus as a main cause of efficacy loss and recommend introducing variability in order to delay it, which is exactly what the randomized scan pattern and the detection-triggered activation of the PEKAN 1 are meant to do, even if this was not tested on live birds.

3. Device architecture

Functionally, the three primary abstraction blocks are Logic, Control Buffer and Power. The workflow can be summarized as follows: the Logic Block identifies the target using a single board computer (SBC), then relays a detection command to the Control Buffer so that an audio file can be played or the DC/servo motors can be moved, while the solar and battery management system handles power delivery. The diagram in Figure 3 illustrates this sequence of actions:

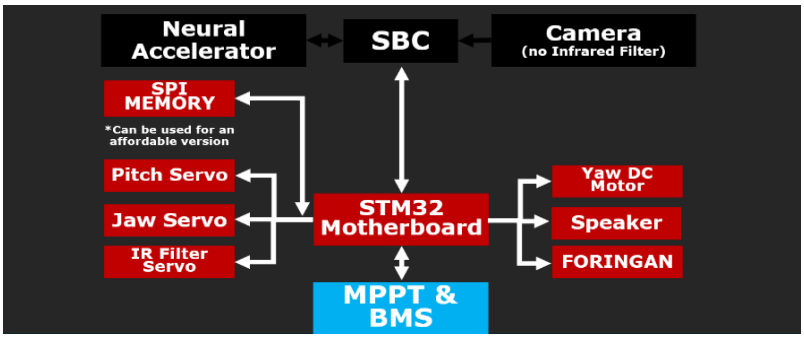


Figure 3. Simplified working diagram of the PEKAN 1. Background color by block: Logic – black, Control Buffer – red, Power – blue
(Source: Author's own research)

Special components such as the external serial peripheral interface (SPI) memory and the infrared light emitting diodes matrix eye (IR LEDs) – which was called “FORINGAN” – will be discussed later in the article.

3.1. Logic Block (LB)

Due to the requirement for a mature development ecosystem and a well-stocked single board computer, the Raspberry Pi 5 16GB was chosen as the controlling SBC. The neural accelerator was selected from Hailo Technologies' product range, while the camera is a 12 Megapixel Raspberry Pi NoIR V3 module. This combination keeps the system within the Raspberry Pi software ecosystem while adding local hardware-accelerated inference and an infrared-sensitive camera path for night operation (Raspberry Pi Ltd, 2026a; Raspberry Pi Ltd, 2026b; Raspberry Pi Ltd, 2026c).

The neural accelerator has been included to offload the inference workload from the Pi 5. Running heavy models on the CPU alone would increase chip temperature and latency, while lowering the possible frame rate. With the accelerator present, the SBC can focus on camera acquisition, decision logic and communication with the rest of the system. The hardware choice also influenced the model training and deployment workflow: Hailo's toolchain uses compiled HEF files for target deployment, so the trained YOLO model had to be exported and converted into a hardware-specific inference artifact before use (Ultralytics, 2026; Hailo Technologies, n.d.). This narrows the practical model pool to architectures and export paths that the accelerator toolchain can support.

3.2. Control Buffer Block (CBB)

Protecting the Raspberry Pi is the main reason for the Control Buffer Block, an intermediary between high-level decision making and low-level hardware control. In this design, an STM32U3-powered PCB controls the servo motor, drives the 360-degree DC motor, plays or records audio on the external SPI memory, and communicates with the audio amplifier IC. The STM32U375 family was suitable because it provides the required SPI, I2C, UART, timer and 12-bit DAC resources, while the DC motor stage benefits from an H-bridge driver with integrated current regulation (Texas Instruments, 2021; STMicroelectronics, 2026).

Powering the device from a 12 V rail allows the audio amplifier to deliver approximately 12-15 W into a 4-ohm load, which is slightly below the speaker's continuous rating. The TAS5441-Q1 is specified as a 1-channel automotive class-D amplifier with I2C diagnostics and a 22 W output rating under its 14.4 V, 4-ohm test condition, while the selected speaker is rated at 20 W and 94 dB at 1 W/1 m (Texas Instruments, 2023; Visaton, n.d.). Therefore, the theoretical 107 dB value at 1 m is a speaker-side power calculation, not a guarantee that the implemented 12 V amplifier stage reaches the full speaker limit.

Knowing that the sound pressure level (SPL) increases logarithmically with electrical input power (P) in Watts, the theoretical maximum value at 1 meter can be computed using the formula:

$$SPL = 94 + 10\log_{10}(P) \tag{1}$$

Plugging in the maximum recorded speaker power draw of 15 W into the equation, the estimated maximum SPL is approximately 106 dB at 1 m.

Assuming free-field operating conditions and a practical acoustic output of 106 dB at 1 m, the estimated free-field sound pressure at a distance d can be found using the formula:

$$SPL(d) = SPL(1m) - 20\log_{10}(d) \tag{2}$$

Considering 80 dB as a practical acoustic threshold, the maximum theoretical acoustic range of the loudspeaker stage is approximately 19 m under free-field assumptions. However, the complete system response range is limited by the object-detection stage, which reached 9 m in daylight and 4 m at night in the present prototype. The calculations below verify the maximum theoretical acoustic range:

$$SPL(19m) = 106 - 20\log_{10}(19) \quad (3)$$

$$SPL(19m) = 106 - 25.57507 \quad (4)$$

$$SPL(19m) = 80.42dB \quad (5)$$

Saving and playing audio files is possible thanks to the on-board 128 Mbit SPI memory, which corresponds to roughly 16 MB of non-volatile storage. The selected W25Q128JV is a 3 V serial flash memory with standard, dual and quad SPI modes, and its datasheet explicitly lists voice, text and data storage among suitable use cases (Winbond, 2024). Audio files are uploaded in a raw monophonic PCM format, encoded as signed 16-bit little-endian samples at 22.05 kHz. At this quality level, the memory can hold approximately 380 seconds of uncompressed audio. There are two upload paths: a host-side script can transfer data via UART, or the Raspberry Pi can relay chunks to the STM32 over I2C for field updates.

As for the FORINGAN, it is a matrix of 5 parallel strings, each with 3 IR LEDs in series. Each string is powered from the 12 V rail and dimensioned for an approximate forward current of 100 mA, resulting in a theoretical maximum of 500 mA and an estimated electrical input power of 6 W. The SFH 4258S LED family was selected for 850 nm infrared emission, high radiant intensity and a narrow optical spread; in practical terms, the 15-degree half-angle helps concentrate more of the optical power forward instead of dispersing it uniformly across a wide field (ams OSRAM, 2024).

3.3. Power Block (PB)

There are two main components handled at this level: the solar panel and the battery pack. The panel is rated at 130 W, with a nominal voltage of 20.5 V and an open-circuit voltage of 24 V. The battery is a 5S, 15 Ah LiFePO4 pack with two main cables connected to its terminals: the charge/discharge lead and the balance cable.

The Power Block handles MPPT charging, balancing, overcurrent, overvoltage, undervoltage (overdischarge) and short-circuit cases. It uses two specialized integrated circuits: the BQ24650 solar charger for input-voltage-regulated charging, and the BQ76920 battery monitor for cell measurement, balancing and protection control (Texas Instruments, 2020; Texas Instruments, 2022). Further functional details are described in Section 4.

4. Performance evaluation

Within this section, we evaluate the most critical functional and safety aspects of the PEKAN 1, namely: effective object detection range, power draw in day/night mode, passive battery balancing, overcurrent cutoff threshold, overdischarge cutoff threshold, overcurrent recovery threshold, actual battery charge current, and how the MPPT charger responds under insufficient solar radiation. All experiments and measurements were performed manually and with hobby-grade equipment.

4.1. Effective object detection range

The experimental maximal object detection range was defined as the maximal distance from the animatronic pole at which the 3D-printed object resembling a crow could still be detected in at least 3/5 attempts when placed within the camera's visual perimeter. The device keeps spinning until it detects a valid target, at which point it triggers an auditory response. If the model does not detect the crow-like object during the scan, the run is considered a failed attempt. The experimental setup can be seen in Figure 4.



Figure 4. Experimental setup for determining the object detection range
(Source: Author's own research)

The roof of a building was chosen as the experimental location. After several attempts, the maximum satisfactory detection distance during the day was 9 meters, slightly lower than the expected value of 12 meters. At night, the range decreased to 4 meters, as shown in Figure 5. The drop is consistent with the much more demanding imaging conditions created by the available IR illumination and the reflective printed target.



Figure 5. Night vision camera's view with the IR LEDs turned on
(Source: Author's own research)

4.2. Power PCB parameters

The following parameters are strictly related to the PCB handling the solar panel and battery management. Unless otherwise noted, the experimental equipment used to extract the data consisted of a Maxwell MX 25 201 multimeter, a NANKADF Programmable DC Power Supply and an ATORCH DL24P electronic load tester.

4.2.1. Power draw

The baseline operating draw used for the autonomy calculation was approximately 14.1 W – battery voltage: 17.02 V, current: 0.83 A, measured with a multimeter and a current clamp, respectively – with the YOLO11 960 px inference model running. During the night, enabling the FORINGAN IR matrix adds approximately 6 W, bringing the nighttime operating budget to about 20.1 W. This value should be interpreted as a system-level power budget, because the IR contribution is obtained from the LED matrix design current rather than from a separate optical efficiency measurement (ams OSRAM, 2024).

4.2.2. Passive battery balancing

Balancing can only be performed on non-adjacent cells, and the discharge current is set by an external resistor using the following formula:

$$I_{balance} = \frac{V_{cell}}{R_{balance}} \tag{6}$$

Because the BMS IC's internal cell-balancing drivers are used, the design is bound by the 50 mA internal cell-balancing current limit. Texas Instruments also warns that adjacent cells should not be balanced simultaneously, which is why the firmware only enables non-adjacent cells in the same balancing step (Texas Instruments, 2022). At 3.65 V, the maximum voltage for an LFP cell, and with a resistance of 75 ohms per string, the sunk current would be:

$$I_{balance} = \frac{3.65V}{75\Omega} = 48.7mA \tag{7}$$

In the experiment, the cells were intentionally unbalanced, with voltages from cell 1 to cell 5 equal to: 3.44 V, 3.46 V, 3.44 V, 3.37 V and 3.45 V, respectively. Balancing is considered successful when all cells fit within an interval of 30 mV.

The experiment concluded in approximately 52 hours, when all 5 cells satisfied the criteria.

4.2.3. Overcurrent cutoff threshold (OC)

For this experiment, we used the adjustable electronic load. The maximum continuous discharge current can be computed using the formula:

$$I_{trip} = \frac{V_{OCD}}{R_{SENSE}} \tag{8}$$

The overcurrent discharge voltage can be modified in the IC firmware, while the sense resistor remains the external modifiable part. On the current printed circuit board (PCB), the OCD threshold has been set to a nominal value of 3.14 A, obtained from the selected register threshold and the 7 mΩ sensing resistor (Texas Instruments, 2022).

Experimentally, the cut-off current was found to be 2.29 A.

4.2.4. Overdischarge cutoff threshold (ODCHG)

Setting the electronic load's discharge current close to the previously determined cutoff value, the battery was discharged uninterruptedly until the BMS cut the power off. The current firmware uses a pack-level cutoff programmed at 15.6 V, which corresponds to 3.12 V/cell in an all-equal situation; experimentally, the ODCHG cutoff voltage was determined to be 15.54 V.

4.2.5. Overcurrent recovery threshold (OCR)

The OCR is the highest instantaneous current value at which the BMS can start supplying again after an OC event without interrupting. By gradually lowering the current below the OC threshold, the OCR was determined to be 2.20 A.

4.2.6. Actual battery charge current (CHG)

The charge current is set by an external shunt resistor. In the BQ24650, the nominal fast-charge current follows the 40 mV / RSR relationship, meaning that the present 16 mΩ shunt sets a theoretical baseline of 2.5 A (Texas Instruments, 2020). The PCB was designed with enough margin for higher charge currents; in an earlier bench test, the highest recorded charging value was 7.304 A at 18.228 V, equivalent to 133.13 W. That bench test indicated that the power path can tolerate power levels comparable to the nominal output of the selected 130 W solar panel. For the current iteration, however, the baseline charge current has been lowered to a nominal 2.5 A because of the factors discussed in Section 4.2.7. Experimentally, the maximum charge current was determined to be 2.36 A under ample solar radiation and a clear sky.

4.2.7. Insufficient solar radiation case

The MPPT charger should handle cases when solar irradiation is insufficient to assure the practical charging wattage of approximately 43 W, computed using the previously determined CHG value and the 18.228 V charge-regulation voltage. The BQ24650 implements solar charging by regulating its input voltage around a programmed maximum power point, so the panel voltage is expected to influence whether charging is allowed to continue (Texas Instruments, 2020). Older

experiments with an earlier version of the power PCB showed that once the solar panel could no longer supply the PCB's demand, the MPPT IC entered a continuous shutdown and restart cycle. The primary cause was the panel voltage falling below the charge voltage when the charger demanded current, followed by recovery when the load disappeared, which created the visible hiccup pattern.

Nonetheless, recent experiments, using the setup shown in Figure 6, uncovered a critical fact about the previous charging-cycle failure: an improper solder joint on the PCB. After fixing it, the IC did cut off the charging current completely and resumed only when the input voltage rose above approximately 18.3 V, which corresponds to the expected behavior.



Figure 6. Simulating the panel's voltage under different weather conditions using an adjustable bench power supply

(Source: Author's own research)

5. Programming

Regarding programming, there are three firmware levels that must be addressed: the buffer PCB and the Power PCB, both programmed in C, and the Raspberry Pi 5, programmed in Python. This splits the project into low-level protection/control firmware and high-level perception logic. The main working algorithm can be defined as follows:

- The Hailo object detection script is activated and, depending on whether it is day or night, the night vision eye is turned on.
- At startup, the Raspberry Pi tells the STM32 buffer PCB to continuously rotate the DC motor that acts on the slip ring. Additionally, the pitch servo motor position is constantly changed in 5-degree increments within a random time interval, making the scan pattern less predictable.
- Upon a valid detection, the Pi tells the buffer to halt all movements. If the detection persists on the vision screen for at least 1 second, the buffer is commanded to play an audio file stored on the SPI memory at the programmed volume. If the detected object/animal does not move and remains in place after three sequential audio playbacks, the animatronic imposes a 1-3 second guard on rotation. This prevents the device from being stuck in one direction by temporarily ignoring new detections and rotating toward a new view.
- The power PCB works independently of the Pi 5 and the buffer PCB, but the hardware ability to make them communicate is present thanks to an I2C breakout header on the PCB. This was not implemented in the current prototype because the slip ring has only 6 wires, all connected to the BMS output, three for positive and three for negative, due to the high current draw of the assembly and the small wire diameter.

6. Discussion

Within the experiments section, there are several differences between theoretical and practical values. One possible explanation is the existence of unaccounted parasitic elements caused by imperfect trace layout, connector losses and measurement tolerances. Another practical concern is the effect of weather, since the device is meant to remain outdoors for long periods of time. Waterproofing is therefore one of the most critical unresolved aspects. A protective layer of epoxy around the electronics would reduce leakage risk, but it would also increase the mass of the head and could affect the current DC motor's ability to rotate the animatronic, potentially requiring a second reduction stage.

Outdoor operation also requires UV-resistant materials. The current parts have been printed primarily with Polycarbonate (PC), Acrylonitrile Butadiene Styrene (ABS) and Polylactic Acid (PLA). While PC is arguably the most appropriate material for long-term operation under harsh meteorological conditions, PLA was only used as a replacement when the available printer could not properly form gears from harder materials. A better next option would be Acrylonitrile Styrene Acrylate (ASA), which is known for good UV resistance and is generally easier to print than PC, which is highly susceptible to warping when the surrounding temperature is not high enough.

Observing the balancing experiment, cell number 4 had the lowest voltage, meaning that the other cells had to be brought down toward its level. This scenario was chosen on purpose because it allows the balancing of three non-adjacent cells simultaneously: cells 1, 3 and 5. Because adjacent cells must not be balanced at the same time and because the algorithm favors balancing as many cells as possible within a run, cell number 2 is left at the end of the balancing line (Texas Instruments, 2022). A future version of the PEKAN 1 could use active balancing, where extra energy is redistributed from higher-voltage cells to lower-voltage cells instead of being dissipated as heat.

Improving the detection range should be one of the top priorities at this stage. Adding a camera with a higher resolution than the currently used 12 megapixels and further optimizing the visual model for a higher frames-per-second value (FPS) could likely increase the range. Another factor that influences detection is the rotation speed, which, if slowed down, might increase the odds of a valid target being identified.

Another aspect future research should address is the night-time detection range of 4 m and overall accuracy of detection under challenging lighting conditions. One possible solution has been highlighted by Sridhar et al. (2025), suggesting the improvement of images for object detection by means of traditional enhancement techniques. Using algorithms such as Unsharp Masking, Gamma Correction and Histogram Equalization, they successfully improved the image quality of several low-light images from an open dataset. Employing the Laplacian Variance as the evaluation metric, they managed to increase the overall edge sharpness and image clarity considerably (3297.93 before and 16912.66 after enhancement on the reference frame), revealing previously hidden objects such as humans and increasing the visibility of license plates. Thanks to the low processing power demand – unlike other methods such as machine learning-based approaches which require dedicated GPUs – their method could be used and run directly on the lightweight Raspberry Pi 5's CPU without any additional external hardware in order to enhance the detection of otherwise unseen animals under low illumination conditions during intervals such as early dusk throughout the evening. It is highly probable that the single most important element in improving complete-dark vision is the addition of a more powerful IR LED matrix; nevertheless, a higher contrast will likely increase the chance of a correct detection by the model.

It should also be noted that the present evaluation focused on prototype-level technical performance and a crow-like validation target; long-term behavioral effectiveness on live birds was not quantified in this study.

As for the old hiccup cycle, where the MPPT IC kept restarting due to a sudden drop in the input voltage caused by external conditions, such concerns are no longer valid after the solder-joint correction. The PCB could theoretically be configured for a maximum of about 7.3 A of charging

current, but for the current iteration, a more moderate charging power, roughly twice the nominal nighttime system draw, was selected.

Even with the limited field testing of the presented prototype, it is a modern approach to the traditional scarecrow. In their review, Sampath & Perepi (2026) discuss the migration from traditional passive scarecrows to advanced deterrence systems that make use of electrical systems and AI models to trigger a deterrent response. Their proposed framework for a complete health monitoring, crop assessment, nutrient management and surveillance system highlights the possibility of creating a low-cost wildlife deterrence system using edge-computing platforms such as the Raspberry Pi or NVIDIA Jetson Nano. This article follows a very similar approach to their crop surveillance proposal, taking it to a built and measured prototype, in which we make use of the latest generation Raspberry Pi 5 in combination with a neural accelerator hat in order to enable low-cost accurate detection of birds and wildlife in the agricultural industry.

7. Future work

Having so far highlighted the main weak points of the current prototype, there are a number of different aspects a future version should consider. Fixing these items will allow the device to operate under real-world test conditions, such as on a field or an orchard.

To begin with the core detection functionality, a 16-megapixel or higher camera should be mounted, while the object detection model's dataset should be expanded in order to cover various other lighting or environmental conditions. Experimenting with different rotation speeds should provide insights into the ideal rotation speed, balancing reaction time against accuracy of detection.

Furthermore, waterproofing is a must under typical outdoor conditions. The future PEKAN should have a solid epoxy encapsulation over the printed circuit boxes, or, as an alternative to an otherwise rigid and almost irreversible process, incorporate an IP65 or higher rated electronics box in the head, sealing the cables with PG-7 glands.

8. Conclusions

With all of the above being mentioned, it can be concluded that the PEKAN 1 is a promising minimum viable product with clear room for improvement. By improving adverse-weather resilience, replacing the current IR matrix with a more powerful emitter, using a more durable and easier-to-print material for the mechanical parts, and increasing the peak battery charging current by adjusting the corresponding shunt, the PEKAN 1 could become a credible deterrent against crows, ravens and starlings. With a retrained detection model and a different sound library, the same architecture could also be adapted to discourage predators such as foxes or wild boars near gardens, farms or villages close to mountainous regions.

Author contributions

The author confirms sole responsibility for the conceptualization, design, implementation, testing, analysis, writing and revision of the manuscript.

Acknowledgements

This project was developed under the guidance of Prof. Marius Enăchescu, Head of the Department of Electronic Devices, Circuits and Architectures. His continuous support and valuable expertise contributed significantly to the development of this project. The author would also like to thank the sponsors ALIMENT MURFATLAR and AXXIS NOVA RESORT AND SPA for their support, which contributed to the development of the research presented in this article. Lastly, I would like to express my gratitude to everyone who contributed in various ways: Prof. Iulian Năstac, Atanasiu Francisc, Mario-Adelin Ciurea, Cristea Alexandru-Mihai, Anghel Eduard-Alexandru, and Tudor Dospinescu.

Submission received: 02 June 2026; Revised: 12 August 2026; Accepted: 25 August 2026; Published: 30 September 2026.

REFERENCES

ams OSRAM (2024) *SFH 4258S: High Power Infrared Emitter (850 nm).* https://ams-osram.com/products/leds/ir-leds/osram-power-topled-lens-sfh-4258s [Accessed: 31 May 2026].

Beason, R. C. (2004) What can birds hear? In: Timm, R. M. & Gorenzel, W. P. (eds.) *Proceedings of the 21st Vertebrate Pest Conference. Davis, California, University of California*. pp. 92-96. https://escholarship.org/uc/item/1kp2r437 [Accessed: 16 August 2026].

Bishop, J., McKay, H., Parrott, D. et al. (2003) Review of international research literature regarding the effectiveness of auditory bird scaring techniques and potential alternatives. *Department for Environment, Food and Rural Affairs*. https://canadianbirdstrike.ca/review-of-international-research-literature-regarding-the-effectiveness-of-auditory-bird-scaring-techniques-and-potential-alternatives/ [Accessed: 31 May 2026].

Duttenhefner, J. L. & Klug, P. E. (2024) Effective range of auditory frightening devices based on hearing capabilities and antipredator responses of nuisance blackbirds. *Wildlife Society Bulletin*. 48, e1549. https://doi.org/10.1002/wsb.1549.

Gilsdorf, J. M., Hygnstrom, S. E. & VerCauteren, K. C. (2002) Use of frightening devices in wildlife damage management. *Integrated Pest Management Reviews*. 7(1), 29-45. https://doi.org/10.1023/A:1025760032566.

Hailo Technologies (n.d.) *Hailo AI Software Suite*. https://hailo.ai/products/hailo-software/hailo-ai-software-suite/ [Accessed: 31 May 2026].

Hema, N. (2022) Solar powered smart ultrasonic rodent repellent with DTMF and manual control for poultry farms. *International Journal of Progressive Research in Science and Engineering*. 3(4), 115-120. https://journal.ijprse.com/index.php/ijprse/article/view/543 [Accessed: 16 August 2026].

Minnesota Department of Natural Resources (n.d.) *Frightening techniques*. https://www.dnr.state.mn.us/livingwith_wildlife/crows/frightening.html [Accessed: 31 May 2026].

Raspberry Pi Ltd (2026a) *AI HATs.* https://www.raspberrypi.com/documentation/accessories/ai-hat-plus.html [Accessed: 31 May 2026].

Raspberry Pi Ltd (2026b) Camera. https://www.raspberrypi.com/documentation/hardware/camera/picam/ [Accessed: 31 May 2026].

Raspberry Pi Ltd (2026c) *Raspberry Pi computer hardware*. https://www.raspberrypi.com/documentation/hardware/raspberrypi/specs.md [Accessed: 31 May 2026].

Sampath, A. & Perepi, R. (2026) AI-Driven ScarecrowAgriBot framework for enhanced agricultural sustainability. *Romanian Journal of Information Technology and Automatic Control*. 36(1), 35-48. https://doi.org/10.33436/v36i1y202603.

Sridhar, R., Suresh, R. A., Babu, S. & Ravisankar, P. (2025) Improving low-light image quality for object detection and license plate recognition. *Romanian Journal of Information Technology and Automatic Control*. 35(2), 87-98. https://doi.org/10.33436/v35i2y202507.

STMicroelectronics (2026) STM32U375xx: Ultra-low-power Arm Cortex-M33 32-bit MCU datasheet. *DS14861*. Rev. 3, February 2026. https://www.st.com/resource/en/datasheet/stm32u375ce.pdf [Accessed: 31 May 2026].

Texas Instruments (2020) BQ24650 Stand-Alone Synchronous Buck Battery Charge Controller for Solar Power with Maximum Power Point Tracking datasheet. *SLUSA75B*. July 2010, revised January 2020. https://www.ti.com/lit/ds/symlink/bq24650.pdf [Accessed: 31 May 2026].

Texas Instruments (2021) DRV8874-Q1 H-Bridge Motor Driver with Integrated Current Sense and Regulation datasheet. *SLVSF67B.* August 2019, revised January 2021. https://www.ti.com/lit/ds/symlink/drv8874-q1.pdf [Accessed: 31 May 2026].

Texas Instruments (2022) BQ769x0 3-Series to 15-Series Cell Battery Monitor Family for Li-Ion and Phosphate Applications datasheet. *SLUSBK2I*. October 2013, revised March 2022. https://www.ti.com/lit/ds/symlink/bq76920.pdf [Accessed: 31 May 2026].

Texas Instruments (2023) TAS5441-Q1 22-W Analog Input 1-Channel Automotive Class-D Audio Amplifier with Load Dump and I2C Diagnostics datasheet. *SLOSE41C*. April 2020, revised September 2023. https://www.ti.com/lit/ds/symlink/tas5441-q1.pdf [Accessed: 31 May 2026].

Tiwari, D. K. & Ansari, M. A. (2016) Electronic pest repellent: a review. In: *Proceedings of the 2016 International Conference on Innovations in Information, Embedded and Communication Systems (ICIIECS'16)*. pp. 435-439. https://www.researchgate.net/publication/305026367_ Electronic_Pest_Repellent_A_Review [Accessed: 16 August 2026].

Ultralytics (2024) *Ultralytics YOLO11*. https://docs.ultralytics.com/models/yolo11/ [Accessed: 31 May 2026].

Ultralytics (2026) *Hailo export for Ultralytics YOLO models*. https://docs.ultralytics.com/ integrations/hailo/ [Accessed: 31 May 2026].

USDA APHIS (2026) *Wildlife Damage Management Technical Series: Bird dispersal techniques*. https://www.aphis.usda.gov/sites/default/files/Bird-Dispersal-Techniques-WDM-Technical-Series.pdf [Accessed: 31 May 2026].

Visaton (n.d.) *SL 87 XA - 4 Ohm*. https://www.visaton.de/en/products/drivers/fullrange-systems/sl-87-xa-4-ohm [Accessed: 31 May 2026].

Winbond (2024) *W25Q128JV 3V 128M-Bit Serial Flash Memory with Dual/Quad SPI datasheet*. Rev. M, 24 December 2024. https://www.winbond.com/hq/product/code-storage-flash-memory/serial-nor-flash/?partNo=W25Q128JV [Accessed: 31 May 2026].



Andrei FOCA is a second-year student at the National University of Science and Technology POLITEHNICA Bucharest, Faculty of Electronics, Telecommunications and Information Technology. Throughout his activities, he has won five awards at international competitions in his field, most recently first prize in the “Most Creative” category at the Robotics Championship in Oradea. His journey started in October 2022 with a small interactive cardboard robot, and since then, he has developed several well-received projects, gaining valuable experience. He has acquired most of his skills from online sources and books on electronics purchased independently, favoring a hands-on approach over purely theoretical activities and relying on his own efforts to acquire the knowledge necessary to develop his projects.

Andrei FOCA este student în anul al II-lea la Universitatea Națională de Știință și Tehnologie POLITEHNICA București, Facultatea de Electronică, Telecomunicații și Tehnologia Informației. De-a lungul activității sale, a obținut cinci premii la competiții internaționale din domeniul său, cel mai recent fiind premiul I la categoria „Most Creative”, în cadrul competiției Robotics Championship din Oradea. Parcursul său a început în octombrie 2022, cu un mic robot interactiv realizat din carton, iar de atunci a dezvoltat mai multe proiecte apreciate, dobândind o experiență valoroasă. Andrei FOCA și-a dobândit majoritatea competențelor din surse online și din cărți de electronică achiziționate pe cont propriu, preferând o abordare practică în locul activităților pur teoretice și bazându-se pe propriile eforturi pentru a dobândi cunoștințele necesare dezvoltării proiectelor sale.



This is an open access article distributed under the terms and conditions of the
Creative Commons Attribution-NonCommercial-ShareAlike 4.0 International License.